Chapter 6
Hydrogen Storage Performance of Metal Nanoparticle Decorated Multi-walled Carbon Nanotubes

Saratchandra Babu Mukkamala

6.1 Introduction

The progress of a nation is directly related to various developmental activities, i.e., agriculture, industry, transport, and industrialization through consumption of energy. The world is facing the over-consumption of energy due to overwhelming growth of population and changing standard of living [1]. So, the current energy resources are not sufficient to meet the present energy demand. There is a vast difference between advanced countries and under-developed countries in the usage of energy [2]. Rapid development of cities due to industrialization and migration of people from rural to urban areas for employment is the major cause for energy demand. Due to urbanization, majority of the world's population is likely to migrate to the urban areas by 2050 according to UN assessment [3].

In addition to the challenges of meeting the increasing energy demand, there is a severe problem with the emission of hazardous pollutants [4]. CO_2 is the major air pollutant in the environment destroying the livelihood of mankind through greenhouse gas effect [5]. Burning of fossil fuels is the major source of CO_2 emissions and reason for climate change [6]. To tackle the challenges of the future energy demand and environmental pollution, particularly CO_2 emissions, progress in the alternative sources of energy such as ethanol, biodiesel, methanol, and hydrogen is inevitable [7].

Among the renewable energy sources, hydrogen is an ideal energy carrier which is considered for future automotive applications. Hydrogen has high energy density (120 MJ/kg) than petroleum fuels [8, 9]. Water moisture is the end product when hydrogen reacts with oxygen. Economic use, suitable storage medium, and infrastructure are some of the key factors considered for promoting the hydrogen as a fuel

S. B. Mukkamala (✉)
Department of Chemistry, Institute of Science, GITAM (Deemed to be University), Visakhapatnam, A.P. 530045, India
e-mail: smukkama@gitam.edu

S. Kaneko et al. (eds.), *Carbon Related Materials*,
https://doi.org/10.1007/978-981-15-7610-2_6

for substitution to existing fossil fuels. Many investigators reported the significance of hydrogen and its obstacles in commercial applications [10, 11]. Hydrogen is a feasible energy source to fill the gap and perfectly replace the existing fossil fuels. In spite of added advantage, hydrogen fuel has some challenges in onboard vehicle applications such as 300 miles travel range, life time of 1500 cycles, and cost of fuel storage system. The production, storage, and delivery of hydrogen are shown in Fig. 6.1.

Many automobile manufacturers are developing fuel cell vehicles for hydrogen-driven hybrid cars. Reaching the set specific goals of the Department of Energy (DOE) is an uphill task. The 2015 target of the light-duty vehicles with a mileage range of 300 miles is yet to be achieved. Production, storage, and transportation continue to be the major challenge for realization of commercial applications.

The development of an effective and safe hydrogen storage system is a key enabling technology for onboard vehicle applications. The US Department of Energy (DOE) established specific technical targets (6.0 wt% capacity at non-cryogenic conditions) for onboard hydrogen storage systems for hydrogen storage. Storage of hydrogen in stationary power, portable power, and transportation is a crucial technique for the progress of hydrogen-powered fuel cell technologies. Hydrogen storage is widely classified on the basis of physical and chemical processes (Fig. 6.2).

Hydrogen can be stored physically either in gas (high pressure tank, 350–700 bar) or liquid form (cryogenic tank, 77 K). Adsorption on a solid is the key process for the storage of hydrogen at non-cryogenic conditions and moderate pressures. Different sorbents, metal hydrides, metal–organic frameworks (MOFs), porous carbons, nanocones, etc., with necessary modifications could meet the DOE targets [12–14]. The Department of Energy (DOE) has set the targets for hydrogen storage

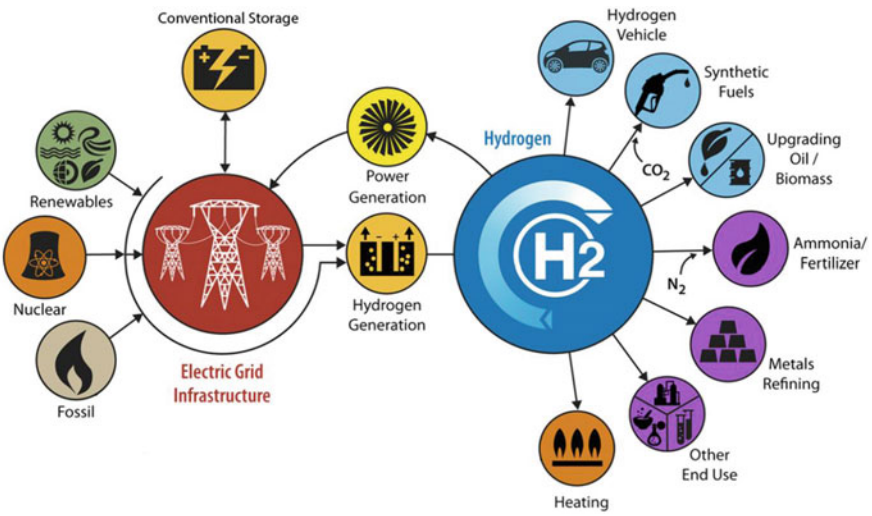

Fig. 6.1 Hydrogen production and applications. *Source* Energy.gov

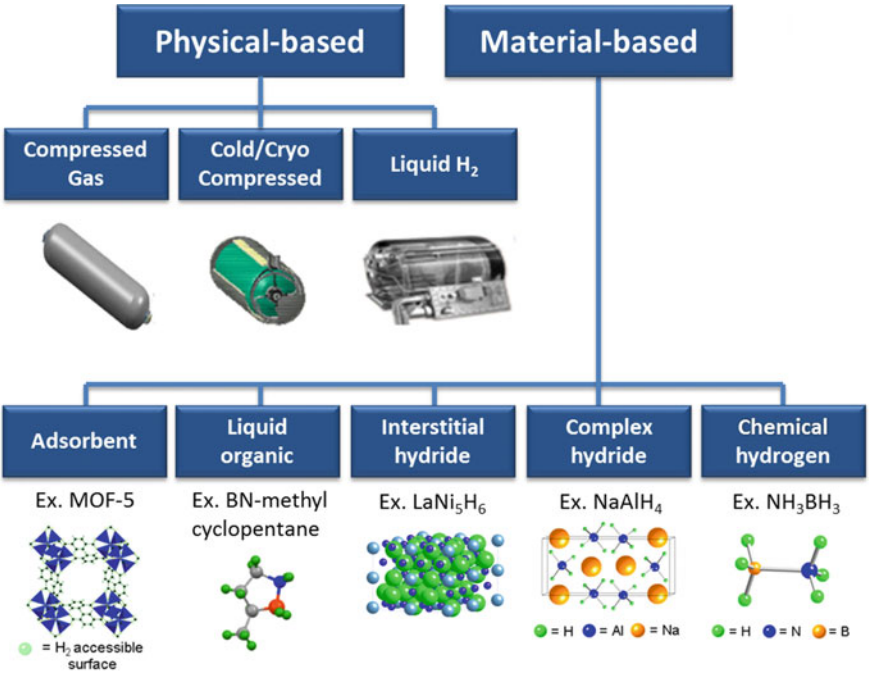

Fig. 6.2 Diverse hydrogen storage methods. *Source* Energy.gov

capacities in terms of volumetric (40 g/L) and gravimetric (5.5 wt%) by 2020 for onboard applications in automobile industry [15]. Carbonaceous materials such as carbon nanotubes (CNTs), graphene, and fullerenes are some of the most promising physical adsorbents for storing hydrogen at non-cryogenic temperatures especially at room temperature [16]. Large surface area, superior chemical and physical properties like hollowness prompt the CNTs as elite entities for promoting hydrogen storage [17–20]. One of the drawbacks of bare CNTs is that the interaction with molecular hydrogen (H_2) is very weak and consequently the uptake of H_2 is not in the appreciable amount. In order to get the high volumetric and gravimetric densities as well as improved binding of CNTs with H_2, numerous studies have been conducted toward enhancement of porosity, surface area, and number of defects by surface functionalization of CNTs [21, 22]. One of the approaches for improving the hydrogen storage efficacy of CNTs is decoration with metal nanoparticles which strengthens the hydrogen–substrate interaction and facilitates the H_2 spillover to CNTs [23–25].

Many studies revealed that the hydrogen storage capacity could be significantly enhanced by incorporating different metals such as Pd, Co, Cu, Fe, Ni, and Ti on MWCNTs at ambient conditions [26, 27]. The hydrogen storage capacity of metal-MWCNTs has been investigated by using an electrochemical hydrogen storage technique. So, after doping the Fe nanoparticles, the hydrogen storage capacity was

enhanced to 0.75 wt% from pristine 0.3 wt% at ambient conditions. Nanocomposites of metal oxides and hydrides also examined for hydrogen uptake. Nanocomposites, MgH_2 and Cr_2O_3, adsorbed 5.2 wt% of hydrogen at 598 K, $LiAlH_4$ and Cr_2O_3 adsorbed 1.9 wt% hydrogen at 448 K [28, 29]. Nickel (Ni) nanoparticles decorated on MWCNTs through functionalization adsorbed 0.87 wt% of hydrogen at 298 K and 100 bar [30]. The hydrogen uptake of MWCNTs had increased 25-folds at 298 K and 16 bar after decorating titanium (Ti) nanoparticles on surface and reached about 2.0 wt% [31]. The spillover effect of Ti increased the H_2 storage ability of MWCNTs. Rather and Hwang have prepared the composite by two different methods, namely ball milling and sputtering, and compared the H_2 storage in the composites prepared from both methods. The H_2 storage was 0.43 and 2.0 wt% for the composites prepared by ball milling and sputtering, respectively, at 298 K and 16 bar. The enhancement of H_2 storage for the composite prepared by the sputtering method is possibly due to the smoother decoration of Ti on the outer surface of the MWCNTs than for that prepared by the ball milling method. The study describes the importance of preparation method in the storage of H_2. Recent reports show that hydrogen storage capacity of MWCNTs had enhanced tenfold at 298 K and ~23 bar after adding cobalt oxide and copper oxide catalyst [32]. The deposition of ultra-fine Co and Cu oxide particles on the outer surfaces of the MWCNTs improved the storage abilities compared to that of pristine MWCNTs. The H_2 storage capacities were 0.8 wt% and 0.9 wt% for Co oxide/MWCNTs and Cu oxide/MWCNTs, respectively, at 298 K and ~23 atm. The spillover mechanism due to embedded Co oxide and Cu oxide on the MWCNTs resulted in the enhancement of storage capacities tenfold for pristine MWCNTs (0.09 wt%) under the same experimental conditions. Studies from the literature showed that experimental conditions such as solvent and metal concentration could play an important role in decorating metal or metal oxide nanoparticles on MWCNTs for uptake of hydrogen [33–36].

6.2 Methods

6.2.1 Functionalization and Synthesis of Metal Decorated MWCNTs

The decoration of multi-walled carbon nanotubes (MWCNTs) with metal/metal oxide nanoparticles is done either by physical mixing through ball milling [37] or chemical process [38]. In contrast to physical method, the chemical method gives reproducible results. Surface modification of carbon nanotube by functionalizing with carboxylic and hydroxyl groups is one of the reported strategies to enhance doping with metal/metal oxide nanoparticles [39–41]. The schematic diagram shows the mechanism for the formation of metal decorated MWCNTs (M@f-MWCNTs) (Fig. 6.3).

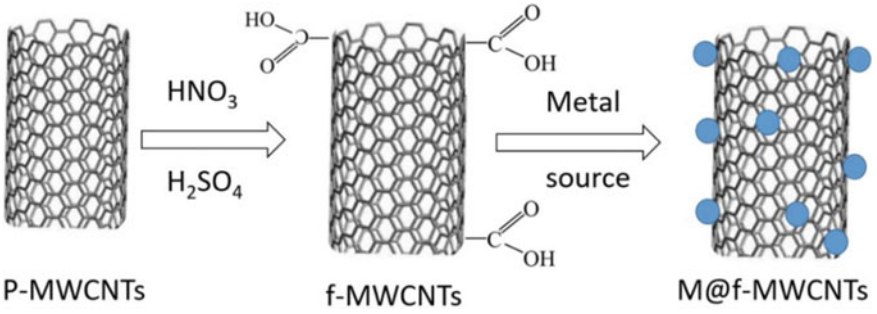

Fig. 6.3 Schematic diagram shows the metal decoration on f-MWCNTs

The raw MWCNTs were placed in a silica crucible and calcined in the furnace at 773–793 K for 2 h followed by treatment with 6.0 M HCl at 368 K for 6 h. Finally, the MWCNTs were washed several times with deionized water until the pH value of the solution became neutral followed by drying overnight at 313 K to get the pristine MWCNT (p-MWCNT). For functionalization of MWCNTs, 0.3 g of the p-MWCNTs and 150 mL of nitration mixture (1:3 HNO_3 and H_2SO_4) were refluxed under magnetic stirring for 48 h. The resulting solid was filtered and washed up to neutral pH, and the sample was dried overnight in vacuum at 313 K. For synthesis of metal oxide nanoparticle decorated f-MWCNTs, 200 mg of carboxylate functionalized MWCNTs (f-MWCNTs) and 0.02 mol [7.36 g of $Ti(NO_3)_4{\cdot}4H_2O$/8.00 g of $Cr(NO_3)_3{\cdot}9H_2O$/8.08 g of $Fe(NO_3)_3$/4.83 g of $Cu(NO_3)_2$/5.94 g of $Zn(NO_3)_2{\cdot}6H_2O$, high metal concentration (HMC)] or 0.01 mol [3.67 g of $Ti(NO_3)_4{\cdot}4H_2O$/4.00 g of $Cr(NO_3)_3{\cdot}9H_2O$/4.04 g $Fe(NO_3)_3$/2.42 g of $Cu(NO_3)_2$/2.97 g of $Zn(NO_3)_2{\cdot}6H_2O$, low metal concentrations (LMC)], were taken in a 500 mL round-bottomed flask. To this, 150 mL distilled water/150 mL distilled water containing 0.5 mL triethyl amine (TEA)/150 mL dimethyl formamide (DMF) was mixed thoroughly and heated at 353 K for 6 h (solution pH of aqueous medium was ~7.0 and TEA medium was ~10.0). The resulting solid was washed till the pH was neutral. The sample was dried overnight in vacuum at 313 K.

The morphology/texture of the obtained compounds p-MWCNTs, f-MWCNT, and M@f-MWCNTs was examined using FEI Quanta 200 FEG scanning electron microscope (SEM) and Philips CM200 transmission electron microscope (TEM). Diffraction patterns were recorded by using PANalytical X'Pert PRO powder X-ray diffractometer with graphite monochromatic CuKα ($\lambda = 1.5406$ Å) radiation at room temperature. The specific surface area was determined according to the Brunauer–Emmett–Teller (BET) method using Quantachrome NOVA 1200e.

The high-pressure hydrogen adsorption measurements for the synthesized materials were conducted on BELSORP-HP (BEL, Japan). Initially, the material was heated thoroughly under dynamic vacuum at different temperatures for long time until the outgas rate was stable in the instrument. After activating the material for long time, the weight of the sample was calculated again and the difference between the two weights could give an idea for the assessment of evacuation of solvent

guest molecules from the pores. Then, the material's hydrogen storage capacity was measured at different temperatures (253 and 298 K) and pressures up to 70 bar. An ultra-pure (99.9999%) helium and hydrogen gases were used for the measurements to get accurate results.

6.2.2 Morphology and Texture

The morphology of the p-MWCNTs, f-MWCNTs, and metal oxide (TiO_2, Cr_2O_3, Fe_2O_3, CuO, and ZnO) decorated MWCNTs (M@f-MWCNTs) has been examined through scanning electron microscopy (SEM) and transmission electron microscopy (TEM). The morphology of p-MWCNTs was examined by SEM is shown in Fig. 6.4a. Tangled tubes with diameters of 20–40 nm of p-MWCNTs were observed. Furthermore, the morphology of MWCNTs before and after carboxylate functionalization was also examined through TEM. The TEM image of p-MWCNTs is shown in Fig. 6.4b. The average diameter of carbon nanotube is 30 nm. Usually, a significant decrease in tube length, change in texture, and/or an opened end-cap structure is observed in functionalized CNT synthesized by chemical oxidation methods. Careful examination of TEM images revealed that both morphology and end-cap structure of carbon nanotubes with the average diameter of CNTs about 30 nm were well-reserved in f-MWCNTs after functionalization (Fig. 6.5). As shown in Fig. 6.5, the inner and outer diameters of MWCNTs were found to be around 7 and 19 nm, respectively.

To identify the optimum conditions required for designing the materials with efficient hydrogen storage properties, a number of chemical reactions were conducted by changing the reaction media (water/amine/DMF) and metal concentration for decorating the carboxylate functionalized MWCNTs with TiO_2 nanoparticles. As shown in SEM and TEM images (Fig. 6.6a, b), TiO_2 nanoparticles of various sizes, about

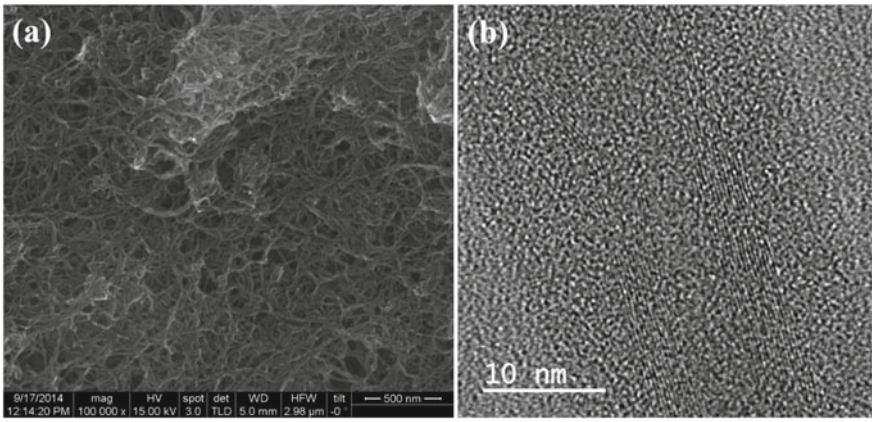

Fig. 6.4 **a** SEM image and **b** TEM images of p-MWCNTs

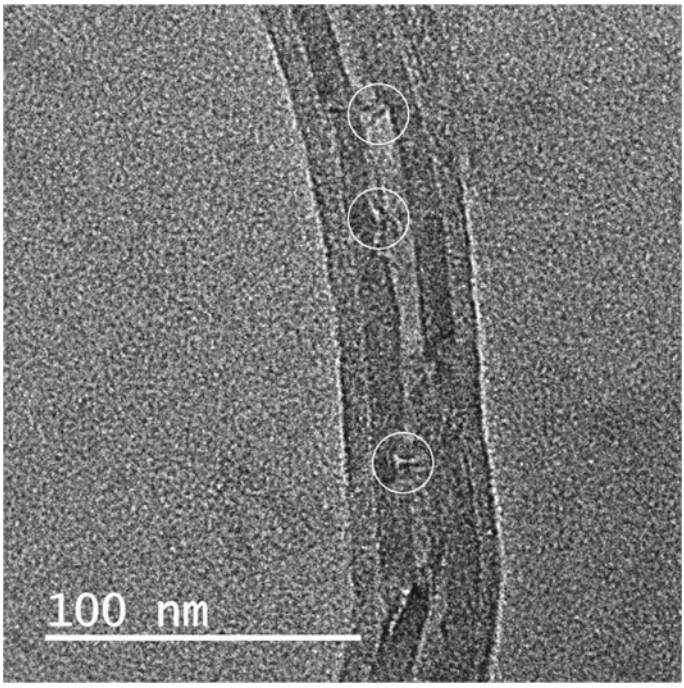

Fig. 6.5 TEM image of f-MWCNTs (encircled: attachment of functional groups on CNT)

50–60 and 10–15 nm, are attached to the outer surface of f-MWCNTs. Elemental composition of TiO_2@f-MWCNTs sample was analyzed through SEM–EDX. As shown in Fig. 6.6c, the presence of C, O, and Ti elements from EDX analysis confirms the presence of the dopant, titanium oxide nanoparticles (16.0 wt%).

Similarly, the carboxylate functionalized MWCNTs were decorated with nanoparticles of Cr_2O_3 through the soft chemical approach. To identify the optimum conditions required for designing the materials with efficient hydrogen storage properties, a number of chemical reactions were conducted by changing the reacting media and the metal concentration for decorating the carboxylate functionalized MWCNTs. As shown in TEM and SEM images (Fig. 6.7a, b), nanoparticles of Cr_2O_3 about 5–10 nm in size are decorated on the surface of f-MWCNTs. Recently, Chen group [42] reported that Cr_2O_3 nanoparticles with size range from 5 to 10 nm are evenly decorated on the surface of the MWCNTs when synthesized though hydrothermal/annealed at 180 and 500 °C. EDX analysis of Cr_2O_3@f-MWCNTs was shown in Fig. 6.7c. These results showed that the presence of Cr, C, and O content confirms the formation of Cr_2O_3 on f-MWCNTs.

For metal decoration on f-MWCNT to produce Fe_2O_3@f-MWCNTs as well as to identify the optimum conditions for efficient hydrogen sorption properties, a number of chemical reactions were conducted like mentioned above. Figure 6.8a, b depicts

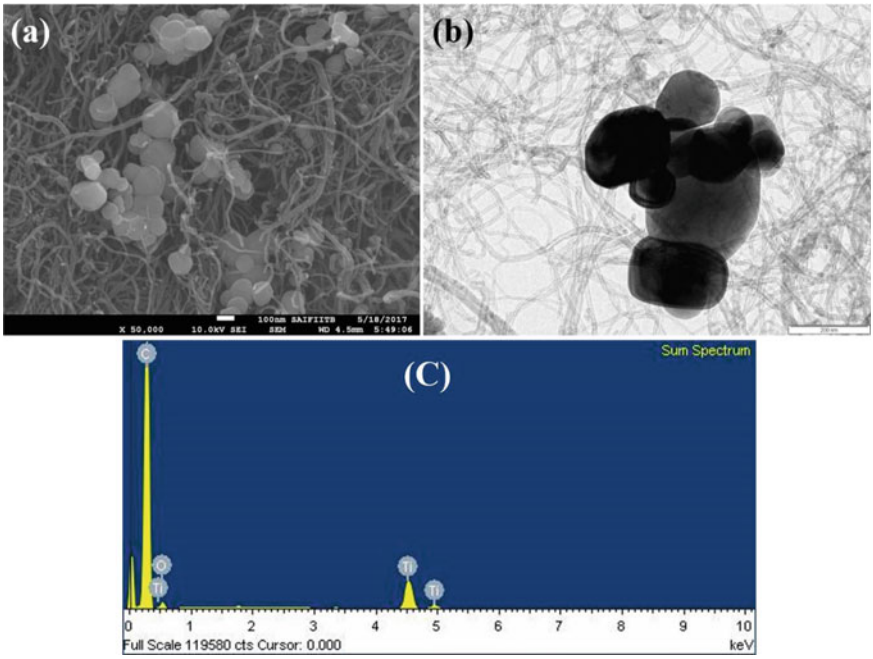

Fig. 6.6 **a** SEM image, **b** TEM image, **c** EDX analysis of TiO_2@f-MWCNTs

the SEM and TEM images of Fe_2O_3@f-MWCNTs. As shown in Fig. 6.8b, 10–20 nm sized nanoparticles of Fe_2O_3 are attached on surface of f-MWCNTs. EDX analysis was also employed to determine the metal content in the synthesized sample (Fig. 6.8c). Our results showed that the amount of Fe_2O_3 doped into the MWCNTs in DMF medium is about 26.83 wt% at higher metal concentration (HMC).

Figure 6.9 depicts the SEM and TEM images of CuO nanoparticle decorated f-MWCNTs. As shown in Fig. 6.9a, b, CuO nanoparticles were attached on the outer walls of the MWCNTs. EDX analysis showed that the amount of CuO doped into the MWCNTs in DMF medium is about 53.95 wt% at HMC (Fig. 6.9c).

Similarly, to identify the optimum conditions required for designing the materials with efficient hydrogen storage properties, a number of chemical reactions were conducted by changing the reaction media and the metal concentration for decorating the carboxylate functionalized MWCNTs with ZnO nanoparticles. Figure 6.10a, b shows SEM and TEM images of ZnO@f-MWCNTs. As shown in Fig. 6.10b, 20–40 nm sized nanoparticles of ZnO are attached on surface of f-MWCNTs. EDX analysis shows the elemental composition of C, O, and Zn which confirmed the presence of the dopant of Zinc oxide nanoparticles (Fig. 6.10c). The present study reveals that the quantity of Zn doped on MWCNTs at MHC was about 0.74 wt% and at MLC was about 0.62 wt%.

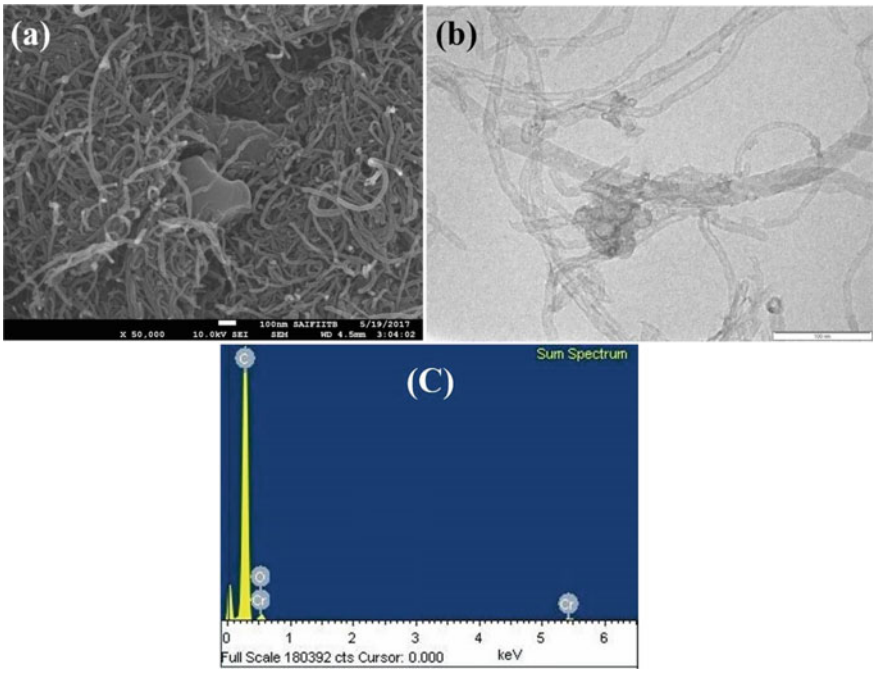

Fig. 6.7 **a** SEM image, **b** TEM image, **c** EDX analysis of Cr_2O_3@f-MWCNTs

6.2.3 Powder XRD Analysis

Powder X-ray diffraction patterns of p-MWCNTs, TiO_2@f-MWCNTs, Cr_2O_3@f-MWCNTs, Fe_2O_3@f-MWCNTs, CuO@f-MWCNTs, and ZnO@f-MWCNTs are shown in Fig. 6.11. The diffraction peaks at 25.4 and 42.9° correspond to (101) and (100) planes of graphite (JCPDS No. 01-0646) (Fig. 6.11a). For TiO_2 decorated MWCNTs (Fig. 6.11b), TiO_2 exists in two phases namely anatase and rutile. The peaks at 24.9, 37.5, 47.7, 53.5, 54.9, and 62.5° correspond to (101), (103), (200), (105), (211), and (204) planes of anatase phase of TiO_2 (major) (JCPDS No. 71-1166). Similarly, the peaks at 27.2 and 35.7 correspond to (110) and (101) planes of rutile phase of TiO_2 (minor) (JCPDS No. 73-1763). The powder XRD pattern of Cr_2O_3@f-MWCNTs is shown in Fig. 6.11c. The diffraction peaks at 18.13°, 27.6°, and 34.2° correspond to (110), (012), and (104) planes of Cr_2O_3 nanoparticles. The peaks at 13.3, 21.8, 36.5, 58.3, 60.9, 62.6° correspond to (111), (220), (311), (511), and (440) planes of iron oxide nanoparticles (Fig. 6.11d). Diffraction peaks at 34.8, 38.1, and 42.6° correspond to (111), (138), and (131) planes of CuO nanoparticles (Fig. 6.11e). The diffraction peaks at 32.0, 34.7, 36.5, 47.7, 56.8, 63.1, 68.1, and 69.2° correspond to (100), (002), (101), (102), (110), (103), (112), and (201) planes of ZnO nanoparticles (JCPDS No. 36-1451) (Fig. 6.11f).

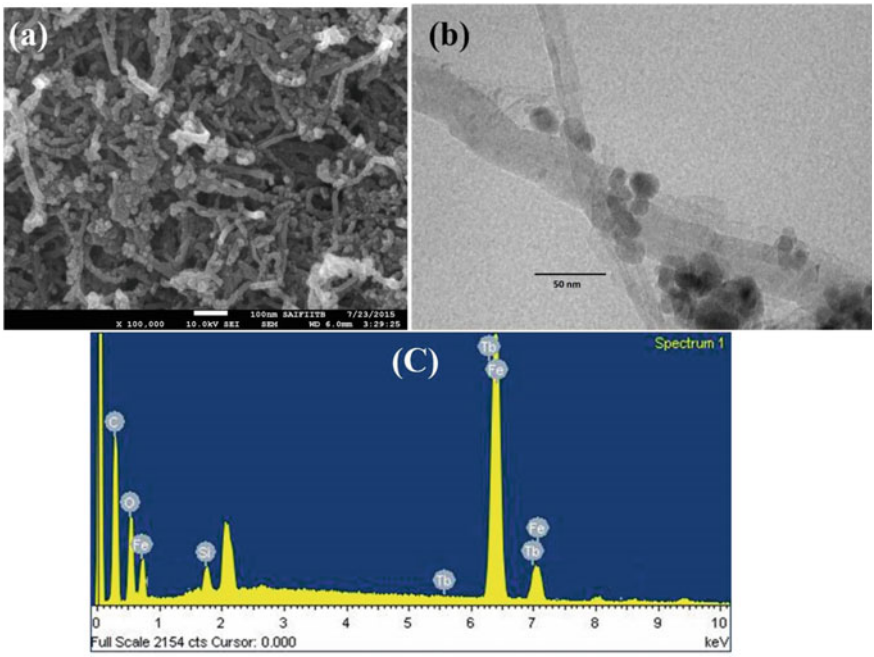

Fig. 6.8 **a** SEM image, **b** TEM image, **c** EDX analysis of Fe_2O_3@f-MWCNTs

6.2.4 Surface Area

The BET specific surface area of p-MWCNTs, f-MWCNTs, and metal decorated MWCNTs was determined by N_2 absorption measurements at 77 K. The surface area of MWCNTs may be influenced by various factors such as tube size, impurities, and surface functionalization (Fig. 6.12). The surface area of p-MWCNTs and f-MWCNTs were 360 and 236 m^2/g. This decrease in surface area is due to blocking of pores by COOH functional groups after surface functionalization of p-MWCNTs. The surface area was further reduced to 229, 212, and 14 m^2/g for TiO_2@f-MWCNTs prepared in water, amine, and DMF, respectively, after metal decoration on f-MWCNTs. Due to the blocking of pores by metal nanoparticles, the surface area is further decreased. The surface area of Cr_2O_3@f-MWCNTs prepared in water, amine, and DMF is 213, 196, 12 m^2/g, respectively. The surface area of Fe_2O_3@f-MWCNTs prepared in water, amine and DMF is 201, 206, and 18 m^2/g, respectively. The surface area of CuO@f-MWCNTs prepared in water, amine, and DMF is 226, 160, and 6 m^2/g, respectively. The surface area of ZnO@f-MWCNTs prepared in water, amine, and DMF is 218, 210, and 17 m^2/g, respectively. A low surface area observed in all cases of metal decorated MWCNTs prepared in DMF media is due to restriction of N_2 access by solvent molecules in the pores of CNTs.

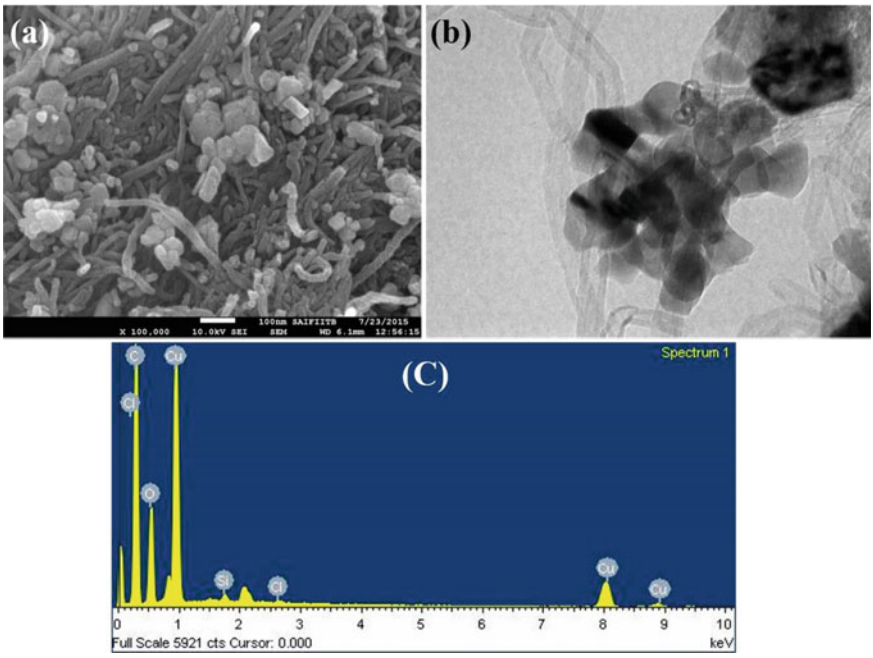

Fig. 6.9 **a** SEM image, **b** TEM image, **c** EDX analysis of CuO@f-MWCNTs

6.3 Hydrogen Storage Property

The hydrogen sorption/uptake capacity of as synthesized compounds were examined volumetrically using high-pressure sorption analyzer BELSORP-HP at non-cryogenic temperatures, i.e., 253 and 298 K. Hydrogen storage capacity of the p-MWCNTs, f-MWCNTs, and M@f-MWCNTs is presented in Table 6.1.

The hydrogen adsorption capacities of TiO_2 decorated MWCNTs along with pristine and functionalized ones were measured volumetrically at 253 and 298 K at moderate pressures of 70 bar. As hydrogen adsorption was reversible in all the samples, the desorption curves have not been shown in Fig. 6.13. The excess sorption isotherms of all the samples display a linear trend typical for monolayer adsorption on porous materials. It was observed that the hydrogen adsorption capacities of pristine and carboxylate functionalized MWCNTs at 253 K and 70 bar pressure are 0.3 and 0.09 wt%, respectively. At 298 K, the hydrogen adsorption capacities of pristine and COOH-MWCNTs are 0.12 and 0.06 wt%, respectively. TiO_2@f-MWCNTs prepared at LMC in water, triethylamine, and DMF adsorbed 0.20, 0.31, and 0.42 wt% of hydrogen (Fig. 6.13a), whereas TiO_2@f-MWCNTs prepared at HMC adsorb 0.67, 0.87, and 1.35 wt% (Fig. 6.13b), respectively, at 253 K. This result indicates that the hydrogen sorption properties drastically increase on increasing the TiO_2 nanoparticle content on the surface of f-MWCNTs. Under the LMC, a linear trend was observed in all the samples. Type III isotherm was observed for the TiO_2@f-MWCNTs prepared

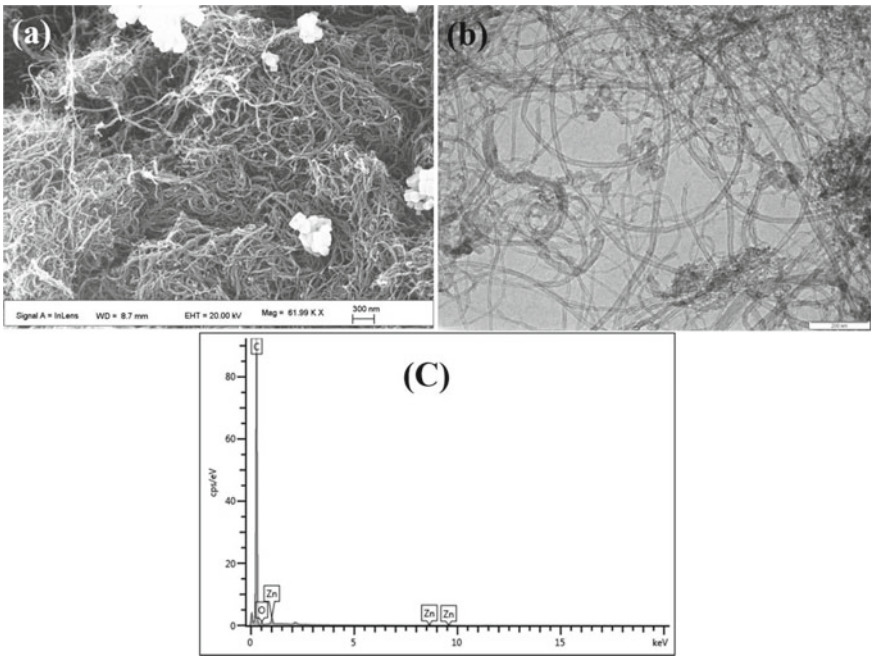

Fig. 6.10 **a** SEM image, **b** TEM image, **c** EDX analysis of ZnO@f-MWCNTs

at LMC in water and DMF due to multilayer formation. Figure 6.13c shows that the hydrogen adsorption isotherms recorded at 298 K for TiO_2@f-MWCNTs prepared at LMC in water, triethylamine, and DMF indicated 0.13, 0.17, 0.22 wt% adsorption. Similarly, TiO_2@f-MWCNTs prepared at HMC under the aforementioned reaction conditions adsorbed 0.31, 0.46, and 0.50 wt% of hydrogen (Fig. 6.13d).

The hydrogen adsorption capacities of Cr_2O_3@f-MWCNTs along with pristine and functionalized ones (p-MWCNTs, f-MWCNTs) were measured volumetrically at 253 and 298 K at moderate pressures of 70 bar. Hydrogen excess sorption isotherms for Cr_2O_3@f-MWCNTs prepared at different metal concentrations (high metal concentration (HMC) and low metal concentration (LMC)) in three different solvents, i.e., water, triethyl amine (TEA), and DMF. Cr_2O_3@f-MWCNTs prepared at (LMC) in water, triethyl amine, and DMF at 253 K adsorbs 0.18, 0.20, and 0.31 wt% of hydrogen (Fig. 6.14a) whereas Cr_2O_3@f-MWCNTs prepared at (HMC) adsorb 0.31, 0.46, and 0.52 wt% (Fig. 6.14b) of hydrogen, respectively. Figure 6.14c shows that the hydrogen adsorption isotherms recorded for Cr_2O_3@f-MWCNTs prepared at (LMC) in water, triethyl amine, and DMF at 298 K indicated 0.13, 0.16, and 0.17 wt% adsorption. Similarly, Cr_2O_3@f-MWCNTs prepared at (HMC) in the above-mentioned reaction conditions adsorbed 0.22, 0.31, and 0.45 wt% of hydrogen (Fig. 6.14d).

The hydrogen storage capacity of Fe_2O_3@f-MWCNTs prepared in water, triethyl amine (TEA), and DMF, at low metal concentration (LMC) was 0.14, 0.18, and

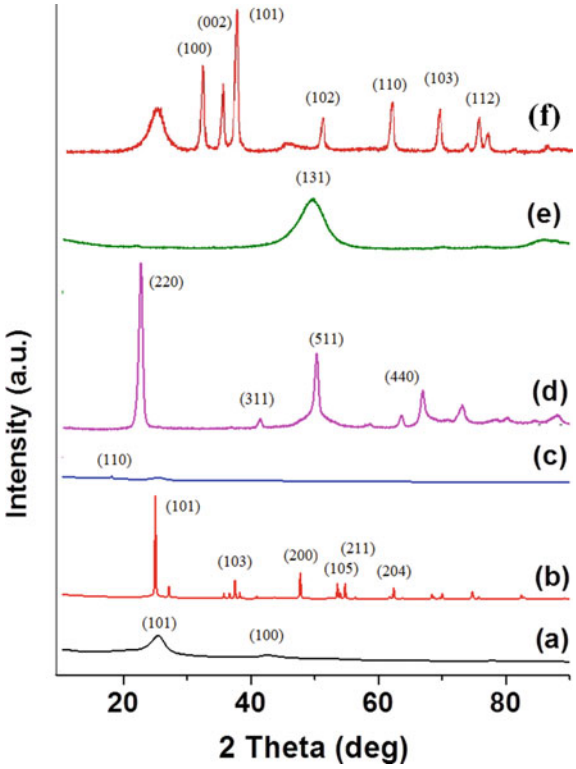

Fig. 6.11 Powder XRD patterns of **a** f-MWCNTs, **b** TiO_2@f-MWCNTs, **c** Cr_2O_3@f-MWCNTs, **d** Fe_2O_3@f-MWCNTs, **e** CuO@f-MWCNTs, **f** ZnO@f-MWCNTs

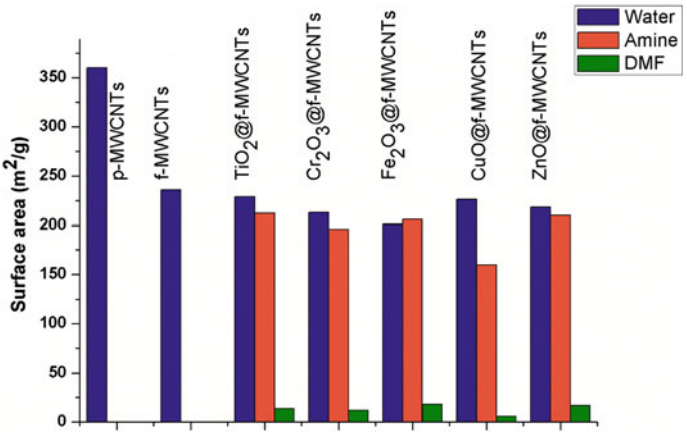

Fig. 6.12 Surface area of p-MWCNTs, f-MWCNTs, and M@f-MWCNTs

Table 6.1 Hydrogen storage capacity of metal decorated MWCNTs

Sample	H_2 storage at 253 K and 70 bar (wt%)			H_2 storage at 253 K and 70 bar (wt%)		
	Medium of sample prepared			Medium of sample prepared		
	Water	Amine	DMF	Water	Amine	DMF
Mg@f-MWCNTs	0.14[a] 0.3[b]	0.25[a] 0.55[b]	0.5[a] 0.67[b]	0.12[a] 0.18[b]	0.17[a] 0.3[b]	0.2[a] 0.45[b]
TiO_2@f-MWCNTs	0.20[a] 0.67[b]	0.31[a] 0.87[b]	0.42[a] 1.35[b]	0.13[a] 0.31[b]	0.17[a] 0.46[b]	0.22[a] 0.50[b]
Cr_2O_3@f-MWCNTs	0.18[a] 0.31[b]	0.20[a] 0.46[b]	0.31[a] 0.52[b]	0.13[a] 0.22[b]	0.16[a] 0.31[b]	0.17[a] 0.45[b]
Fe_2O_3@f-MWCNTs	0.14[a] 0.31[b]	0.18[a] 0.50[b]	0.21[a] 0.55[b]	0.13[a] 0.25[b]	0.14[a] 0.31[b]	0.18[a] 0.39[b]
CuO@f-MWCNTs	0.17[a] 0.39[b]	0.21[a] 0.50[b]	0.39[a] 0.68[b]	0.13[a] 0.31[b]	0.18[a] 0.46[b]	0.31[a] 0.50[b]
ZnO@f-MWCNTs	0.17[a] 0.47[b]	0.19[a] 0.51[b]	0.31[a] 0.87[b]	0.12[a] 0.31[b]	0.17[a] 0.50[b]	0.22[a] 0.67[b]

[a]LMC—Low metal concentration
[b]HMC—High metal concentration

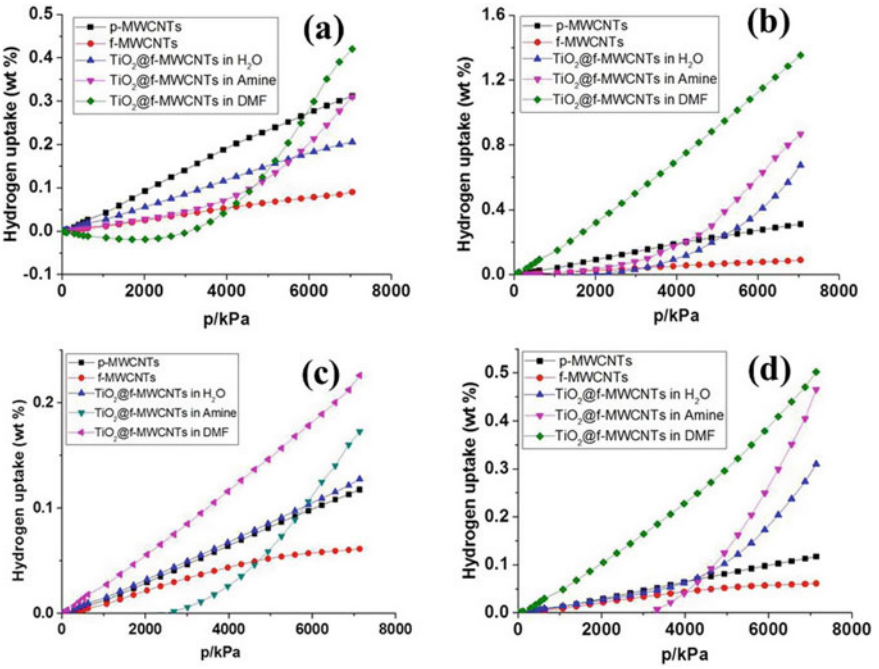

Fig. 6.13 Hydrogen uptake capacities of p-MWCNTs, f-MWCNTs, TiO_2@f-MWCNTs (**a**) at 253 K and LMC (**b**) at 253 K and HMC (**c**) at 298 K and LMC (**d**) at 298 K and HMC

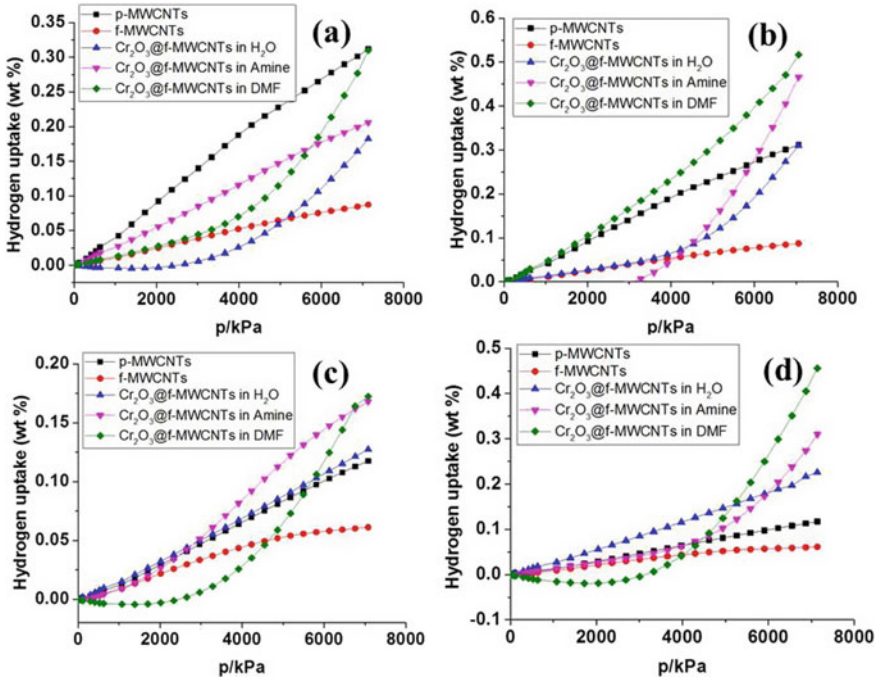

Fig. 6.14 Hydrogen uptake capacities of p-MWCNTs, f-MWCNTs, Cr_2O_3@f-MWCNTs (**a**) at 253 K and LMC (**b**) at 253 K and HMC (**c**) at 298 K and LMC (**d**) at 298 K and HMC (Reproduced with permission from Indian Chemical Society)

0.21 wt%, respectively, at 253 K (Fig. 6.15a), whereas that of prepared at higher metal concentration (HMC) as shown in Fig. 6.15b was 0.31, 0.50, and 0.55 wt%, respectively, at the same temperature, i.e., at 253 K. It was observed that the storage capacity doubled on decorating the surface of CNTs with more iron oxide nanomaterial. The hydrogen storage capacity of Fe_2O_3@f-MWCNTs prepared in water, triethyl amine (TEA), and DMF at low metal concentration (LMC) were 0.13, 0.14, and 0.18 wt%, respectively, at 298 K (Fig. 6.15c). The three materials prepared at high metal concentration (HMC) adsorbed 0.25, 0.31, and 0.39 wt%, respectively, at similar temperature (Fig. 6.15d).

The hydrogen adsorption isotherms of CuO@f-MWCNTs, prepared in water, triethylamine, and DMF, recorded at 253 and 298 K at different metal concentrations (LMC and HMC) are examined. The p-MWCNTs, f-MWCNTs, and CuO@f-MWCNTs prepared water, triethyl amine, and DMF media at LMC adsorbed 0.17, 0.21, and 0.39 wt% of hydrogen (Fig. 6.16a) whereas that prepared at HMC adsorbed 0.39, 0.5, and 0.68 wt% of hydrogen, respectively, at 253 K (Fig. 6.16b). The hydrogen adsorption isotherms of CuO@f-MWCNTs, prepared in the above-mentioned three media, i.e., water, triethyl amine, and DMF, recorded at 298 K are shown in Fig. 6.16c, d. CuO@f-MWCNTs prepared at MLC showed 0.13, 0.18,

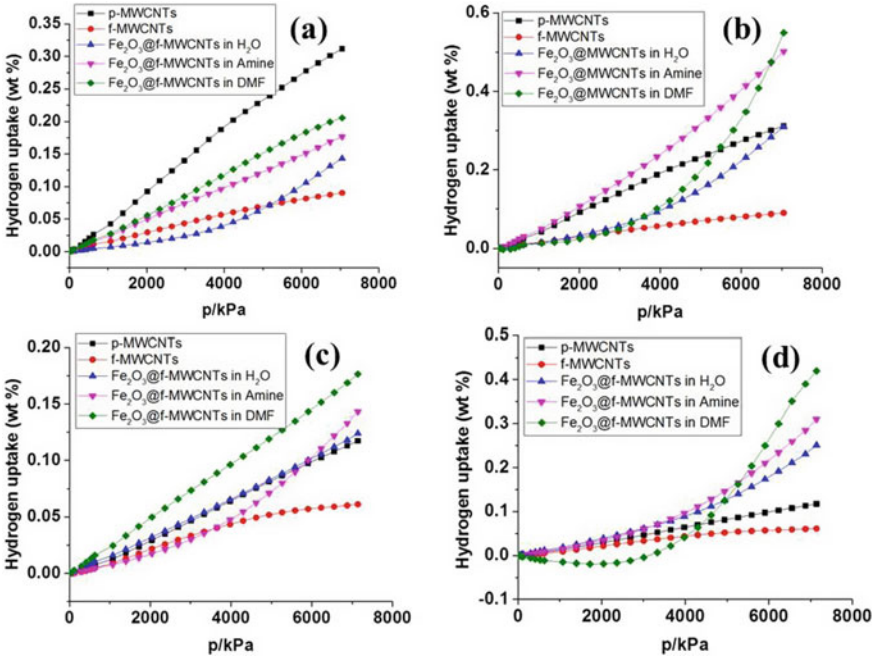

Fig. 6.15 Hydrogen uptake capacities of p-MWCNTs, f-MWCNTs, Fe_2O_3@f-MWCNTs (**a**) at 253 K and LMC (**b**) at 253 K and HMC (**c**) at 298 K and LMC (**d**) at 298 K and HMC (Reproduced with permission from Elsevier)

and 0.31 wt% of hydrogen adsorption, respectively, whereas that prepared at HMC exhibited 0.31, 0.46, and 0.50 wt% of hydrogen adsorption, respectively, at 298 K. The linear isotherm in most of the reactions confirms the monolayer adsorption.

ZnO@f-MWCNTs prepared at LMC in water, triethylamine, and DMF adsorb 0.17, 0.19, and 0.31 wt% of hydrogen (Fig. 6.17a), whereas ZnO@f-MWCNTs prepared at HMC adsorb 0.47, 0.51, and 0.87 wt% (Fig. 6.17b), respectively, at 253 K. This result indicates that the hydrogen sorption properties drastically increase on increasing the ZnO nanoparticle content on the surface of f-MWCNTs. Under the LMC, a linear trend was observed in all the samples. Type III isotherm was observed for the ZnO@f-MWCNTs prepared at LMC in water and DMF due to multilayer formation. Figure 6.17c shows that the hydrogen adsorption isotherms recorded at 298 K for ZnO@f-MWCNTs prepared at LMC in water, triethylamine, and DMF indicated 0.12, 0.17, 0.22 wt% adsorption. Similarly, ZnO@f-MWCNTs prepared at HMC under the aforementioned reaction conditions adsorbed 0.31, 0.50, and 0.67 wt% of hydrogen (Fig. 6.17d). One of the reaction media, DMF, a polar aprotic solvent plays an important role in uniform loading and decoration of ZnO nanoparticles on the surface of MWCNTs. Due to this reason, high storage of hydrogen was observed in the case of ZnO@f-MWCNTs prepared in DMF solvent. Also, the

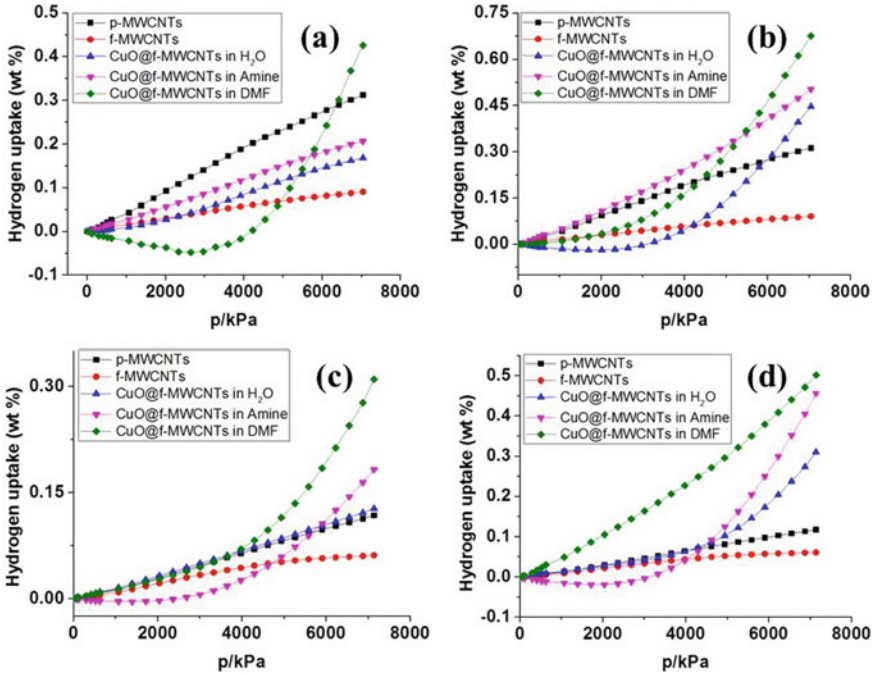

Fig. 6.16 Hydrogen uptake capacities of p-MWCNTs, f-MWCNTs, CuO@f-MWCNTs (**a**) at 253 K and LMC (**b**) at 253 K and HMC (**c**) at 298 K and LMC (**d**) at 298 K and HMC (Reproduced with permission from Elsevier)

adsorption capacity significantly increased at 253 K as compared to that observed at 298 K.

6.3.1 Hydrogen Storage Via Spillover Mechanism

Spillover is an important mechanism to identify the hydrogen adsorption on surface of adsorbents (Fig. 6.18). According to this mechanism, molecular hydrogen adsorbs initially on metal and dissociates later as atomic hydrogen which subsequently migrates to spillover receptor, CNT and enhances the hydrogen storage. The binding energy is the key parameter for ideal adsorption of hydrogen. The essential binding energy for effective hydrogen storage lies between 0.2 and 0.4 eV. In this study, the binding energy calculated for the release of hydrogen was between 0.42 and 0.56 eV. Thus, the hydrogen is attached to the adsorbent by in weak chemical binding rather than chemisorption binding, which requires a larger binding energy (1–10 eV) [43, 44].

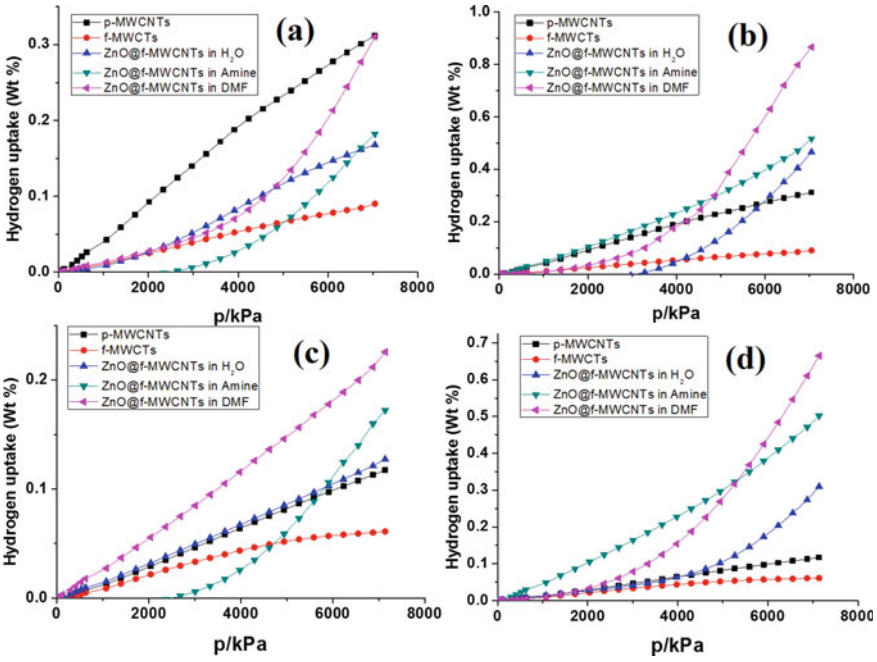

Fig. 6.17 Hydrogen uptake capacities of p-MWCNTs, f-MWCNTs, and ZnO@f-MWCNTs (**a**) at 253 K and LMC (**b**) at 253 K and HMC (**c**) at 298 K and LMC (**d**) at 298 K and HMC (Reproduced with permission from Royal Society of Chemistry)

6.3.2 Cyclic Performance of Adsorption/Desorption of Hydrogen

Cyclic adsorption/desorption performance of hydrogen is the key to evaluate the stability and reusability of material for onboard vehicle applications [26, 45, 46]. So, the selected materials have been examined for multi-cycle test to study the stability and reusability. Every cycle starts with the full evacuation of the chamber to remove the remaining hydrogen. Multi-cycles of adsorption/desorption of hydrogen on the surface of the copper nanoparticle decorated MWCNTs (CuO@f-MWCNTs) which are prepared in DMF media have been examined at 298 K. The adsorption/desorption isotherm is stabilized after 5 cycle measurements and loss in hydrogen storage capacity of about 2.0% was noticed (Fig. 6.19).

Similarly, multi-cycles of adsorption/desorption of hydrogen on the surface of the ZnO nanoparticle decorated MWCNTs (ZnO@f-MWCNTs) which are prepared in triethyl amine media were also examined at 298 K. As shown in Fig. 6.20, the adsorption and desorption isotherm is stabilized after 5 cycle measurements and loss in hydrogen storage capacity of about 6.0% was noticed [36]. So, CuO@f-MWCNTs and ZnO@f-MWCNTs display stable adsorption/desorption of hydrogen.

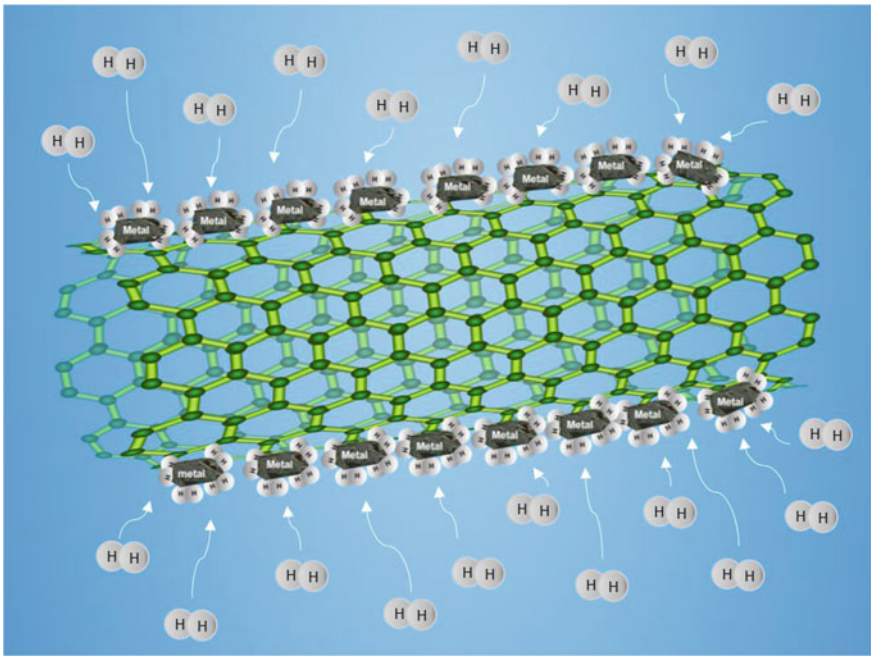

Fig. 6.18 Spillover mechanism of hydrogen storage

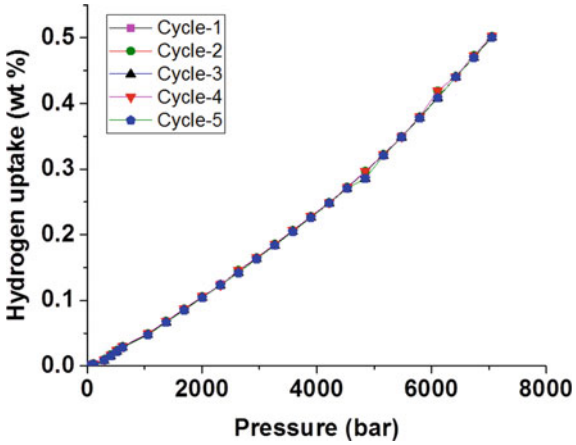

Fig. 6.19 Cyclic life performance of CuO@f-MWCNTs at 298 K

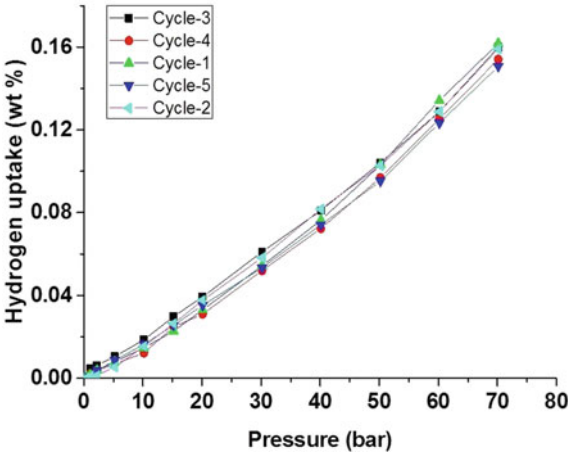

Fig. 6.20 Cyclic life performance of ZnO@f-MWCNTs at 298 K. (Reproduced with permission from Royal Society of Chemistry)

6.4 Conclusions

In conclusion, a substance-based hydrogen storage system using MWCNTs has been investigated. Among carbon materials, carbon nanotubes (SWCNTs and MWCNTs) are actually one of the most promising components for hydrogen storage because of their cage-like structure, high surface area, substantial pore volume, chemical steadiness, and ease of synthesis. The morphology of the synthesized samples was examined using scanning electron microscopy (SEM) and transmission electron microscopy (TEM). One of the biggest issues is usually to fill the cylindrical structure of CNTs with metals and gases. To acquire the substantial volumetric and gravimetric densities as well as better binding of H_2 to CNTs, many studies had been conducted to design effective methods for surface functionalization of CNTs using organic functional groups like carboxyl or hydroxyl to augment porosity and volume of defect. Among the strategies for bettering, the hydrogen storage usefulness of CNTs is decoration with metal nanoparticles, which will strengthen the hydrogen–base interaction and facilitates the H_2 spill to CNTs. The hydrogen storage measurements were conducted at different temperatures and pressures. The decorated metal/metal oxide decoration of nanoparticles is said to raise hydrogen storage capacity through spillover mechanism. Metal nanoparticles on CNTs dissociate the molecular hydrogen and spill it over to CNTs. In this direction, the hydrogen storage capacity of TiO_2, Cr_2O_3, Fe_2O_3, CuO, and ZnO decorated MWCNTs was examined under different experimental conditions such as variable metal concentrations (low metal concentration and high metal concentration) and solvents (water, triethylamine, and DMF) at non-cryogenic temperatures and moderate pressures.

References

1. P. Kennedy, *Preparing for the Twenty-First Century* (Vintage Publications, 2011)
2. J. Rifkin, *The Hydrogen Economy: The Creation of the Worldwide Energy Web and the Redistribution of Power on Earth*, 1st edn. (TarcherPerigee Publications, 2003)
3. E.S. Cassedy, P.Z. Grossman, *Introduction to Energy: Resources, Technology, and Society*, 2nd edn. (Cambridge University Press, Cambridge, 2017)
4. P.J. Crutzen, The "anthropocene", in *Earth System Science in the Anthropocene* (Springer, Berlin, Heidelberg, 2006)
5. R. Gelbspan, *The End of Nature and Beyond. Global Warming and Political Power* (Sage, 2005)
6. A. Demirbas, Potential applications of renewable energy sources, biomass combustion problems in boiler power systems and combustion related environmental issues. Prog. Energy Combust. Sci. **31**, 171–192 (2005)
7. A.K. Mohanty, M. Misra, L.T. Drzal, Sustainable bio-composites from renewable resources: opportunities and challenges in the green materials world. J. Polym. Environ. **10**, 19–26 (2002)
8. K. Mazloomi, C. Gomes, Hydrogen as an energy carrier: prospects and challenges. Renew. Sustain. Energy Rev. **16**, 3024–3033 (2012)
9. R.A. Patricio, A.D. Sales, E.M. Sacramento, L.C. de Lima, T.N. Veziroglu, Wind hydrogen energy system and the gradual replacement of natural gas in the State of Ceará—Brazil. Int. J. Hydrogen Energy **37**, 7355–7364 (2012)
10. S. Chaudhuri, J.T. Muckerman, First-principles study of Ti-catalyzed hydrogen chemisorption on an Al surface: a critical first step for reversible hydrogen storage in $NaAlH_4$. J. Phys. Chem. B **109**, 6952–6957 (2005)
11. C.K. Ngaw, C.E. Zhao, V.B. Wang, S. Kjelleberg, T.T.Y. Tan, Q. Zhang, S.C.J. Loo, A graphene/carbon nanotube biofilm based solar-microbial fuel device for enhanced hydrogen generation. Sustain. Energy Fuels **1**, 191–198 (2017)
12. J.O. Abe, A.P.I. Popoola, E. Ajenifuja, O.M. Popoola, Hydrogen energy, economy and storage: review and recommendation. Int. J. Hydrogen Energy **44**, 15072–15086 (2019)
13. A.A. EL Barbary, Hydrogen storage on cross stacking nanocones. Int. J. Hydrogen Energy **44**, 20099–20109 (2019)
14. A. Joakim, G. Stefan, Large-scale storage of hydrogen. Int. J. Hydrogen Energy **44**, 11901–11919 (2019)
15. DOE, *U.S. Department of Energy—Hydrogen Storage* (2018). https://energy.gov/eere/fuelcells/hydrogen-storage
16. G.E. Froudakis, Nanotubes & nanostructures. Mater. Today **14**, 7–8 (2011)
17. M. Baro, P. Nayak, T.T. Baby, S. Ramaprabhu, Green approach for the large-scale synthesis of metal/metal oxide nanoparticle decorated multiwalled carbon nanotubes. J. Mater. Chem. A **1**, 482–486 (2013)
18. Z. Lei, Z. Yinan, L. Dongfang, L. Heng, Z. Jianxun, C. Peng, L. Wanqiang, Enhanced electrochemical hydrogen storage performance of $Ti_{49}Zr_{26}Ni_{25}$ alloy by doping with Pd nanoparticles deposited MWCNTs. Solid State Sci. **94**, 138–144 (2019)
19. X.L. Ling, Y.Z. Wei, L.M. Zou, S. Xu, Preparation and characterization of hydroxylated multi-walled carbon nanotubes. Colloid Surf. A **421**, 9–15 (2013)
20. S.Z. Mortazavi, P. Parvin, A. Reyhani, R. Malekfarc, S. Mirershadi, Hydrogen storage property of laser induced Pd nanoparticle decorated multi-walled carbon nanotubes. Int. J. Hydrogen Energy **34**, 4243–4255 (2009)
21. W. Song, C. Jeon, M. Kim, Y.T. Kwon, D.S. Jung, S.Y. Kim, The decoration of multi-walled carbon nanotubes with metal nanoparticles of uniform size using MeV electron beam irradiation. Carbon **49**, 1692–1698 (2011)
22. H. Xiao, S.H. Li, J.X. Cao, First-principles study of Pd-decorated carbon nanotube for hydrogen storage. Chem. Phys. Lett. **483**, 111–114 (2009)

23. S.W. Hwang, S. Rather, M. Naik, C.S. Soo, K.S. Nahm, Hydrogen uptake of multiwalled carbon nanotubes decorated with Pt–Pd alloy using thermal vapour deposition method. J. Alloy Compd. **480**, L20–L24 (2009)
24. M.R. Naresh, S. Rajashabala, R. Kannan, Hexagonal boron nitride (h-BN) nanoparticles decorated multi-walled carbon nanotubes (MWCNT) for hydrogen storage. Renew. Energy **85**, 387–394 (2016)
25. A. Reyhani, S.Z. Mortazavi, S. Mirershadi, A.N. Golikand, A.Z. Moshfegh, H_2 adsorption mechanism in Mg modified multi-walled carbon nanotubes for hydrogen storage. Int. J. Hydrogen Energy **37**, 1919–1926 (2012)
26. A. Reyhani, S.Z. Mortazavi, S. Mirershadi, A.Z. Moshfegh, P. Parvin, A.N. Golikand, Hydrogen storage in decorated multiwalled carbon nanotubes by Ca Co, Fe, Ni, and Pd nanoparticles under ambient conditions. J. Phys. Chem. C **115**, 6994–7001 (2011)
27. Z. Xiaojie, L. Zhe, Z. Xiangjun, L. Heng, S. Jing, S. Zhongmin, L. Wanqiang, Z. Jianxun, Improved electrochemical hydrogen storage properties of $Ti_{49}Zr_{26}Ni_{25}$ quasicrystal alloy by doping with Pd and MWCNTs. Int. J. Hydrogen Energy (2019). https://doi.org/10.1016/j.ijhydene.2019.01.103
28. M. Polanski, J. Bystrzycki, R.A. Varin, T. Plocinski, M. Pisarek, The effect of chromium (III) oxide (Cr_2O_3) nanopowder on the microstructure and cyclic hydrogen storage behavior of magnesium hydride (MgH_2). J. Alloys Compd. **509**, 2386–2391 (2011)
29. R. Ud-din, Q. Xuanhui, L. Ping, L. Zhang, M. Ahmad, Hydrogen sorption improvement of $LiAlH_4$ catalyzed by Nb_2O_5 and Cr_2O_3 nanoparticles. J. Phys. Chem. C **115**, 13088–13099 (2011)
30. Y.J. Han, S.J. Park, Influence of nickel nanoparticles on hydrogen storage behaviors of MWCNTs. Appl. Surf. Sci. **415**, 85–89 (2017)
31. S.U. Rather, S.W. Hwang, Comparative hydrogen storage study on titanium-MWCNTs composite prepared by two different methods. Int. J. Hydrogen Energy **41**, 18114–18120 (2016)
32. S.U. Rather, Hydrogen uptake of cobalt and copper oxide-multiwalled carbon nanotube composites. Int. J. Hydrogen Energy **42**, 11553–11559 (2017)
33. M. Konni, S.B. Mukkamala, Hydrogen uptake behavior of Cr_2O_3 nanoparticle decorated f-MWCNTs at non-cryogenic temperatures. J. Ind. Chem. Soc. **95**, 393–397 (2018)
34. M. Konni, N. Narayanam, A.S. Dadhich, S.B. Mukkamala, Effect of reaction media on hydrogen sorption properties of Mg decorated MWCNTs. Fuller. Nanotub. Carbon Nanostruct. **23**, 782–787 (2015)
35. M. Konni, A.S. Dadhich, S.B. Mukkamala, Impact of surface modifications on hydrogen uptake by Fe@f-MWCNTs and Cu@f-MWCNTs at non-cryogenic temperatures. Int. J. Hydrogen Energy **42**, 953–959 (2017)
36. M. Konni, A.S. Dadhich, S.B. Mukkamala, Solvent induced surface modifications on hydrogen storage performance of ZnO nanoparticle decorated MWCNTs. Sustain. Energy Fuels **2**, 466–471 (2018)
37. S.U. Rather, K.S. Nahm, Hydrogen uptake of high energy ball milled nickel-multiwalled carbon nanotube composites. Mater. Res. Bull. **49**, 525–530 (2014)
38. R. Yu, L. Chen, Q. Liu, J. Lin, K. Tan, S. Choon Ng, H.S.O. Chan, G.Q. Xu, T.S. Andy Hor, Platinum deposition on carbon nanotubes via chemical modification. Chem. Mater. **10**(3), 718–722 (1998)
39. J. Aziziani, D.C. Khoei, H. Tahermansour, K. Yadollahzadeh, V. Georgakilas, Functionalization of carboxylated multi-walled carbon nanotubes with 1, 4-phenylendiamine phenylisocynate. Fuller. Nanotub. Carbon Nanostruct. **19**, 753–760 (2011)
40. B. Fernandez-d'Arlas, A. Eceiza, Functionalization of multi-walled carbon nanotubes with urethane segments and their interaction with solvents and a polyurethane elastomer. J. Nanopart. Res. **16**, 2166–2175 (2013)
41. V. Georgakilas, A. Bourlinos, D. Gournis, T. Tsoufis, C. Trapalis, A. Mateo-Alonso, M. Prato, Multipurpose organically modified carbon nanotubes: from functionalization to nanotube composites. J. Am. Chem. Soc. **130**(27), 8733–8740 (2008)

42. B. Chen, Y. Wang, C. Li, L. Fu, X. Liu, Y. Zhu, L. Zhang, Y. Wu, A Cr_2O_3/MWCNTs composite as a superior electrode material for supercapacitor. RSC Adv. **7**, 25019–25024 (2017)
43. K.K. Gangu, S. Maddila, S.B. Mukkamala, S.B. Jonnalagadda, Characteristics of MOFs MWCNTs and graphene mediated materials for hydrogen storage: a review. J. Energy Chem. **30**, 132–144 (2019)
44. D. Silambarasan, M. Kanmani, M. Jeyanthinath, T.R. Ravindran, V. Vasu, Investigation of hydrogen storage in MWCNT–TiO_2 composite. Phys. E Low Dimens. Syst. Nanostruct. **80**, 207–211 (2016)
45. S.S. Kaye, A. Dailly, O.M. Yaghi, J.R. Long, Impact of preparation and handling on the hydrogen storage properties of Zn_4O (1,4-benzenedicarboxylate)$_3$ (MOF-5). J. Am. Chem. Soc. **129**, 14176–14177 (2007)
46. Z. Zhang, S. Xian, Q. Xia, H. Wang, Z. Li, J. Li, Enhancement of CO_2 adsorption and CO_2/N_2 selectivity on ZIF-8 via post synthetic modification. AIChE J. **59**, 2195–2206 (2013)